Film Formation from Polymer Solution Using Inkjet Printing Method

Masayuki Kaneda, Hirotaka Ishizuka, Yousuke Sakai, and Jun Fukai
Dept. of Chemical Engineering, Kyushu University, Fukuoka 819-0395, Japan

Shigekazu Yasutake
Dept. of Chemistry and Biochemistry, Graduate School of Engineering, Kyushu University, Fukuoka 819-0395, Japan

Atsushi Takahara
Institute for Materials Chemistry and Engineering, Kyushu University, Fukuoka 819-0395, Japan

DOI 10.1002/aic.11154
Published online March 19, 2007 in Wiley InterScience (www.interscience.wiley.com).

The factors determining the thin-film shape from an evaporating polymer solution droplet are experimentally studied. The polystyrene/xylene droplets, whose diameter is controlled in the range of 30–100 μm with the mass fraction of 0.5–3.0 wt % are ejected onto a lyophobic substrate. The droplet on the substrate results in an axisymmetric or nonaxisymmetric ring-like/dot-like film. The film configuration is dominated by the evaporation rate and the film symmetry is governed by the local pinning time at the periphery. Various relationships are also found among the evaporation rate, pinning time, wetting diameter, and average solute concentration of which the nondimensionalization pronounces explicit relationships and similarity. © 2007 American Institute of Chemical Engineers *AIChE J,* 53: 1100–1108, 2007
Keywords: film configuration, evaporation rate, pinning time, solute mass fraction, inkjet printing

Introduction

Inkjet printing is well known by the consumer as paper printing devises. This device can eject small sized droplets directly onto a target, and a variety of industrial applications such as an organic light emitting device, polymer electroluminescent device, microlens and integrated circuits, etc., are being studied because of its characteristics.[1–5] These ink-jet related devices require quality film formation after the evaporation. That is, the thickness profile of the thin film and its uniformity are key factors for engineering applications, and related studies have been done. Shimoda et al.[5] reported the different shapes of the film based on the different stage velocity during evaporation. De Gans and Schubert[6] examined the use of a dilute solution to fabricate the well-defined polymer structures. The result of their reports is that the evaporation rate of the solvent may be the dominant factor for the film thickness profiles and its uniformities. However, the relationship between the evaporation rate and the film uniformities is semi-empirical and has not been studied in detail in terms of the transport phenomenon. Furthermore, the association of the evaporating process, detailed film shape and borderlines of the evaporation rate between the dot-like and ring-like film have not been fully discussed.

In this article, the drying process of a polymer solution droplet on a lyophobic surface has been experimentally studied. First, the effect of the drying process on the distortion of the polymer film is investigated. Second, the pinning of the

Correspondence concerning this article should be addressed to J. Fukai at jfukai@chem-eng.kyushu-u.ac.jp.

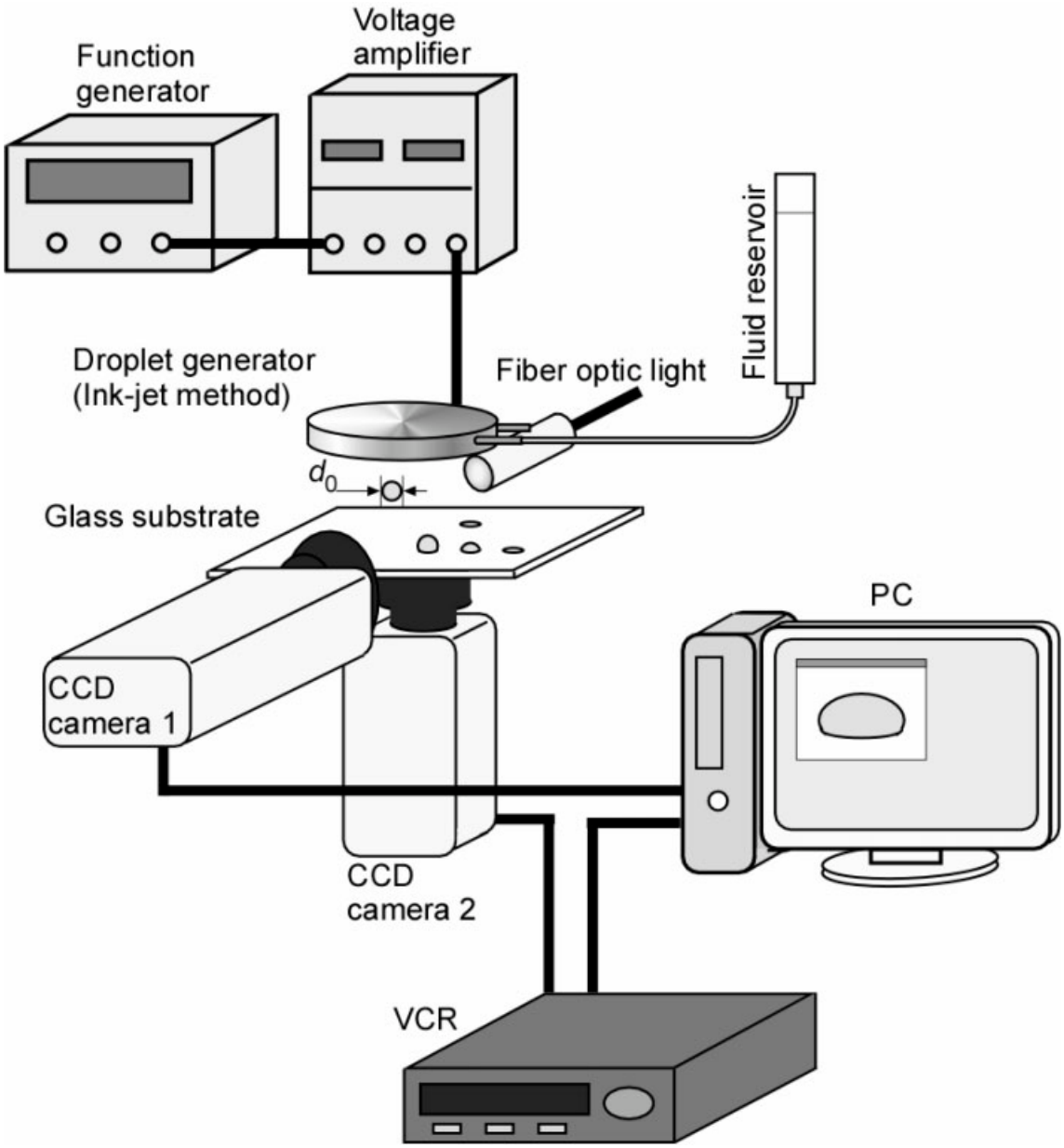

Figure 1. Experimental setup.

contact line is characterized using dimensionless parameters. Last, the factors determining the film configuration are discussed based on considerations of the transport phenomena.

Experimental

Figure 1 shows the experimental schematics. The inkjet droplet generator, which contains a piezo-ceramic transducer, is equipped with a multi-axis micrometer that controls the vertical distance to the substrate of 0.3–1.0 mm and the horizontal adjustment during the droplet ejection. The evaporation rate of the solvent can be controlled by the distance between the nozzle and the substrate because the partial pressure of the solvent around the droplet is sensitive to the width of this clearance. The droplet diameter d_0 is controlled in the range of 30–100 μm by a function generator and a voltage amplifier connected to the droplet generator. Droplets are ejected every second from the generator nozzle to the substrate.

The substrate is made of transparent glass and its surface is chemically modified with a fluoroalkylsilane ($C_6F_{13}(CH_2)_2Si(OCH_3)_3$) monolayer by chemical vapor adsorption, which makes the surface lyophobic.[7] The fluid reservoir supplies the polystyrene/xylene solution to the droplet generator and the mass fraction of the solute is prepared between 0.5 and 3.0 wt %. All experiments were carried out at room temperature. The substrate temperature is maintained at the same temperature as the room. The deposited droplet is recorded using two CCD cameras (30 fps) from the side and bottom views. The instantaneous periphery, wetting diameter, and the height of the droplet are extracted from the recorded video, and then the contact angle is calculated based on the

Table 1. Physical Properties of the Polystyrene/Xylene Solution

	Polystyrene Fraction, wt %			
	0	0.5	3.0	5
Viscosity, 10^{-3} Pa s	0.58	0.87	2.41	4.32
Surface tension, 10^{-3} N/m	28.0	28.0	28.0	28.2

spherical cap. After the drying is finished, the polystyrene films are formed on the substrate. The three-dimensional images of films are obtained using the Keyence VK-8500 laser microscope.

The physical properties of the solutions at certain mass fractions are shown in Table 1. The viscosity was measured by a Brookfield viscometer, LVDV-II, and the surface tension by a Kyowa Interface Science, CBVP-Z. The viscosity increases with the mass fraction but the surface tension is not affected.

Results and Discussions

Local pinning time and film symmetry

A typical evaporating process of a polystyrene/xylene droplet is represented in Figure 2 by the transient contact angle ψ_c and the wetting diameter d_c. First, the wetting diameter decreases until the contact line is pinned at nearly 3.5 s. The contact angle during this process decreases from 65° to 60°. The decrease in it for several other experiments in our group was no greater than 10°.[8] Accordingly, a constant contact angle will be assumed in some of the calculations described later. After the contact line is pinned, the contact angle decreases faster than the previous process and finally the evaporation finishes leaving a thin film.

The visual images of the representative experimental runs are shown in Figure 3. Their initial mass fraction and diameter are 3.0 wt % and 80 μm, respectively. The instantaneous contact line during evaporation [Figure 3a], the resulting thin film shapes [Figure 3b] and their contours [Figure 3c] are represented herein. The images of the instantaneous contact line are recorded every second, which are alternately distinguished by white and black stripes. The innermost peripheries in Figure 3a roughly correspond to those in Figure 3c.

In some experimental runs such as A1-A4 of Figure 3a, the center of the wetting area moves in an arbitrary direction during evaporation. No tendency or repeatability was observed in the direction of the displacement. Whereas, in cases A5-A7, the wetting area concentrically shrinks with time. These experimental runs are carried out under the same conditions, and we cannot predict whether the wetting area moves or not. The horizontal level of the substrate is carefully adjusted by a level vial at every experimental run so that the gravity does not affect the wetting area movement. The size of the droplet is much smaller than the capillary length and effect of gravity is negligible. Thus, the wetting area movement may happen due to the local solvent pressure around the droplet[5] and/or the small nonhomogeneous substrate roughness.

In Figure 3c, A1, A2, and A7 yield symmetric films while others deposit biased films after the evaporation. Comparing Figure 3a with 3c, the film symmetry is irrespective of the wetting area movement. For example, A1 and A2 yield symmetric films even though the centers of wetting areas move. A5 and A6 evaporate concentrically but the films form asymmetrically.

To discuss and clarify the mechanism of the film symmetry, the local pinning time t_{pin} along the contact line is measured from the sequence frames of the recorded video, and indicated around the film periphery in Figures 3c. In the case of A1, because of the strong reflection from the droplet surface, the contact line cannot be accurately identified. More comprehensive graphs are shown in Figure 4, in which the normalized local pinning time $t_{pin}/t_{pin,f}$ is plotted along the azimuth. $t_{pin,f}$ represents the final pinning time along the contact line of each experimental run. The films can be categorized into two classes in terms of the film configuration, i.e., a dot-like deposit and ring-like one. The dot-like films are extracted in Figure 4a and the ring-like ones in Figure 4b. For the dot-like films, A2 has a flat distribution and A3 and A4 have peaks at $\theta = 90°$. For the ring-like films, A6 and B2 (not shown in Figure 3, $d_0 = 100$ μm) have fluctuations. These peaks correspond to the biased film configuration shown in A3, A4, and A6 of Figure 3c. This means that the local pinning of the contact line affects the axis symmetry of the film. This can be understood based on the discussion of Deegan et al.[9,10] and Fischer.[11] They reported that convection is induced toward the periphery from the bulk when the contact line is pinned during evaporation. This is due to the moderately enhanced evaporative flux at the edge of the droplet and the fluid flows to compensate for the solvent around the contact line, which is the formation mechanism of the coffee stain (ring-like deposit). This convection holds the film thickness at the periphery and is applicable to our case in which the contact line is locally pinned. In the same manner, we can assume that if the pinning time is locally later than the other part of the contact line, the convection

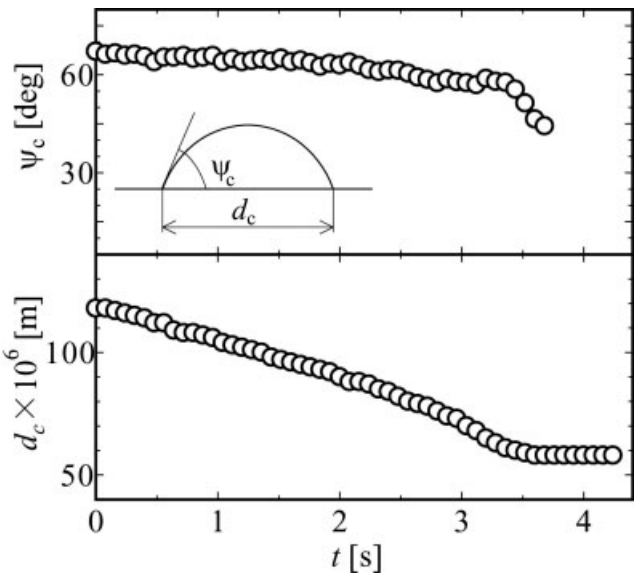

Figure 2. Time variations of the contact angle ψ_c and wetting diameter d_c for the 3 wt % polystyrene/xylene droplet evaporating on the substrate (d_0 = 80 μm).

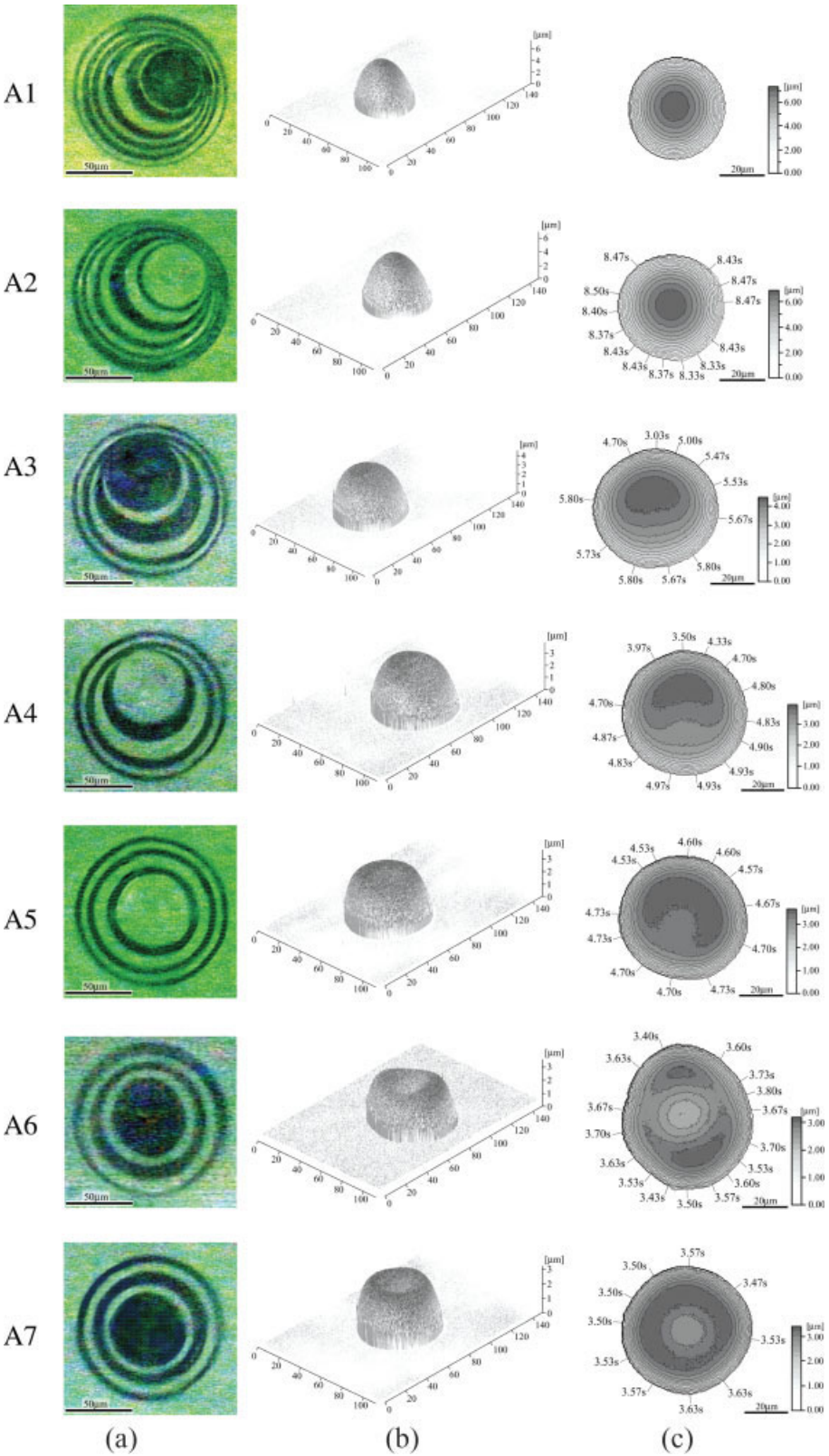

Figure 3. Evaporating behavior and resulted film of 3 wt % polystyrene/xylene droplet with d_0 = 80 μm. (a) The instantaneous droplet periphery at every sec. (b) Three-dimensional image of the thin film after evaporation. (c) The contour plot and the local pining time.

[Color figure can be viewed in the online issue, which is available at www.interscience.wiley.com.]

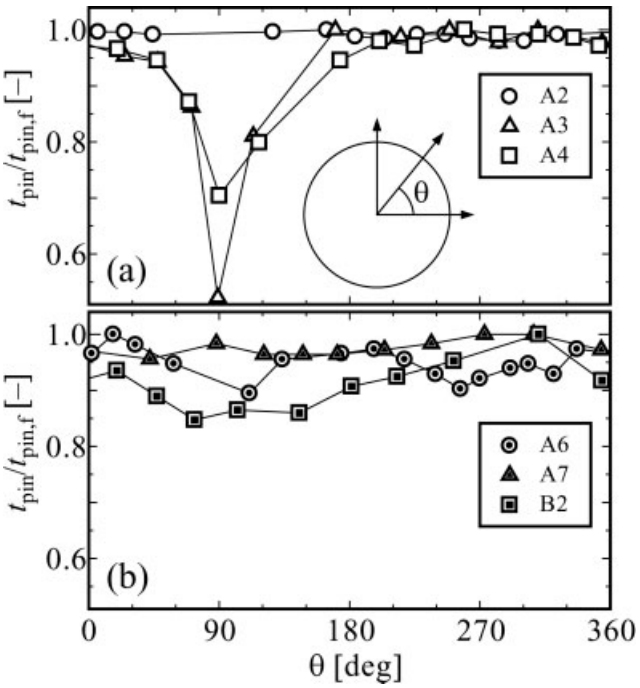

Figure 4. Azimuthal variations of the pinning time normalized with $t_{pin,f}$ for (a) dot-like deposits and (b) ring-like deposits.

toward the contact line may not be induced until it pins, resulting in a lower film thickness. If the pinning time is almost the same along the contact line (A2, A5, and A7), the symmetry of the film thickness is maintained.

The characteristics of the pinning and mass transfer during the receding

In Figures 3 and 4, dot-like deposits are formed for A1–A4 while ring-like deposits are formed for A6–A7. The others are in the transition configuration between them. To discuss the factors dominating the film configuration, the average receding velocity $u_{c,av} = (d_{c0}-d_{c,pin,f})/t_{pin,f}$ is measured for each experimental run. d_{c0} and $d_{c,pin,f}$ represent wetting diameter at $t = 0$ and $t = t_{pin,f}$, respectively. Schematic is shown in Figure 5. Although the evaporation rate from the surface is better to discuss, it changes as the wetting diameter shrinks with time and we employed the receding velocity for the simplification. When the contact angle remains constant while the contact line recedes, the average receding velocity is proportional to the evaporation rate per unit area of the free surface. When considering a slight change in the contact angle, $u_{c,av}$ can be approximately proportional to the evaporation rate. Figures 6 and 7 show the relationship between $u_{c,av}$ and $t_{pin,f}$ and that between $u_{c,av}$ and $d_{c,pin,f}$, respectively. In Figure 6, the lines approximated by the least square method are also presented for three experimental conditions. A good regression between $u_{c,av}$ and $t_{pin,f}$ is found. Dot-like films are formed at the low evaporation rates, while ring-like ones are formed at the high evaporation rates. In Figure 7, $d_{c,pin,f}$ tends to increase as $u_{c,av}$ increases. Thus the $t_{pin,f}$, $d_{c,pin,f}$ and the droplet configuration are found to be somewhat relative to $u_{c,av}$, though, theses relations depend on the initial mass fraction and droplet diameter.

To clarify the relations of these values, the dimensionless wetting diameter, time and velocity are defined as $D = d/d_0$, $\tau = (v_0/d_0^2)t$ and $U = (d_0/v_0)\,u$, respectively. d_0 and v_0 represent initial droplet diameter and initial kinematic viscosity. The average mass fraction at $t_{pin,f}$ is also evaluated from the wetting diameter. Assuming a constant contact angle, the average mass fraction c_{av} at $t_{pin,f}$ is calculated by

$$c_{av.pin,f} = \frac{\rho_{c0}}{\rho_{c,pin,f}}\left(\frac{d_{c0}}{d_{c,pin,f}}\right)^3 c_0 \tag{1}$$

where ρ and c represent the density and the solute fraction of the droplet, respectively.

The results in Figures 6 and 7 are replotted in Figures 8 and 9 according to these definitions. Obviously, the effect of the initial droplet diameter is eliminated and that of the initial solute fraction is pronounced by the non-dimensionalization. Therefore, it is concluded that there is a similarity in the initial droplet size under the present experimental conditions. Furthermore, the borderlines between the dot-like and ring-like film shape in $U_{c,av}$ locate at the same value regardless of the initial solute fraction, which represents that there is another similarity in the transport phenomena.

Because the evaporation rate is proportional to the receding velocity, the following dimensionless regression is applied to the results in Figure 8:

$$\tau_{pin.f} = AU_{c,av}^{B} \tag{2}$$

As shown in Figure 8, $B = -1.07$ and -1.18 for each initial mass fraction is evaluated using the least-square method. Moreover, the dimensionless wetting diameter is given by

$$D_{c.pin,f} = D_{c,0} - \tau_{pin.f}U_{c,av} \tag{3}$$

and the average mass fraction at the pinning can be derived from the following equation.

$$c_{av.pin.f} = \frac{c_0}{\left\{1 - \frac{d_0}{d_{c0}}AU_{c.av}^{B+1}\right\}^3} \tag{4}$$

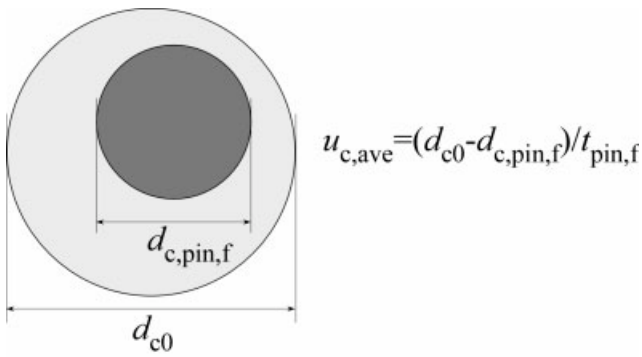

Figure 5. Schematics of d_{c0}, $d_{c,pin,f}$, and $u_{c,ave}$.

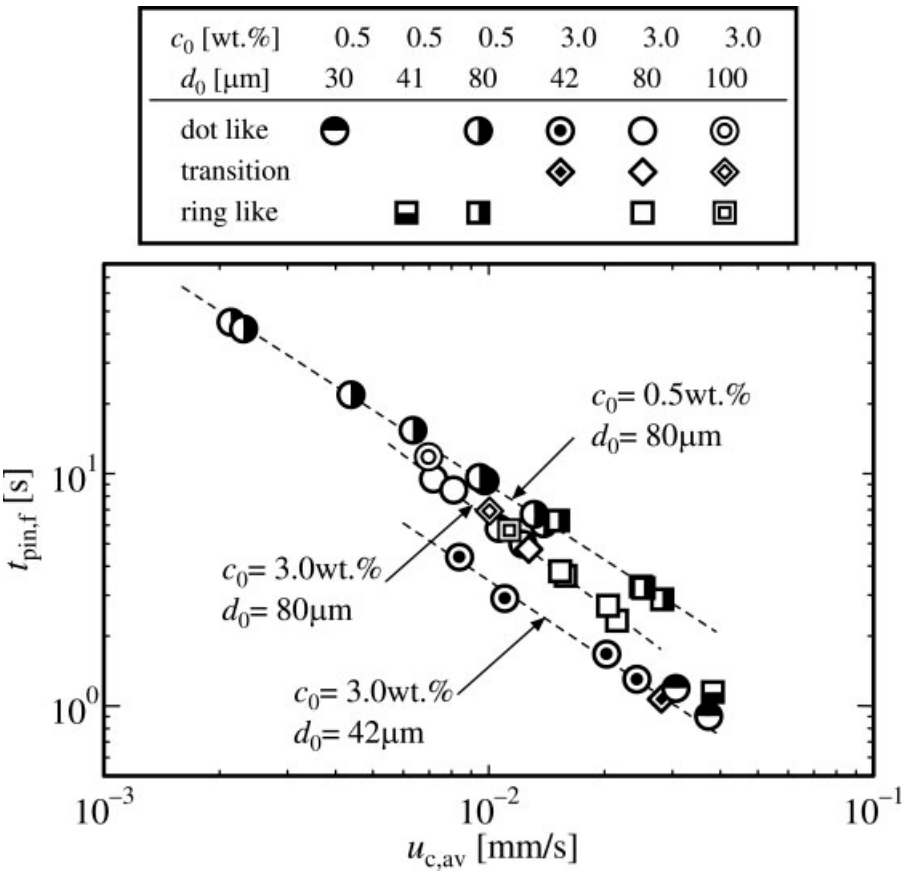

Figure 6. The pinning time vs. average receding velocity.

where,

$$\left(\frac{d_0}{d_{c0}}\right)^3 = \frac{3}{4\sin^3\psi_c}\left(\frac{2}{3} - \cos\psi_c + \frac{1}{3}\cos^3\psi_c\right) \qquad (5)$$

The calculated results from Eqs. 2 and 4, in which the values of A and B identified in Figure 8 are used, are shown in Figures 9 and 10.

The effect of $U_{c,av}$ on $c_{av,pin,f}$ is plotted in Figure 10. Scatter of the results is greater than that in Figures 8 and 9 because the measurement errors in the wetting diameter affect the calculated results by the third power. However, the effect of c_0 on $c_{av,pin}$ seems to be eliminated. As the receding velocity becomes faster, $c_{av,pin}$ becomes smaller. If the solute is perfectly mixed in the droplet, the pinning occurs at the constant solute fraction and the calculated curves are inde-

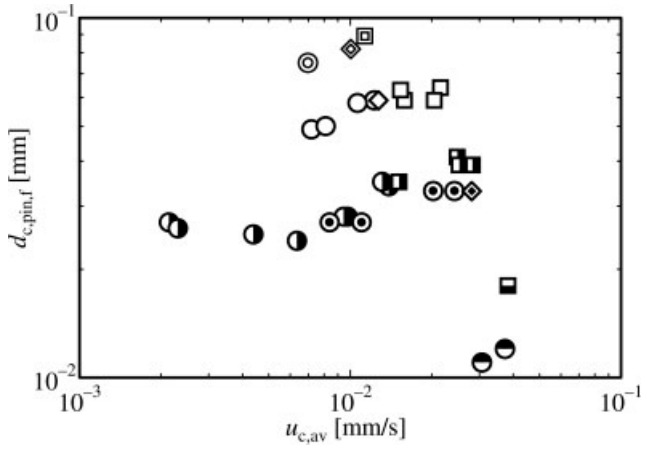

Figure 7. Wetting diameter at $t = t_{pin,f}$ vs. the receding velocity.

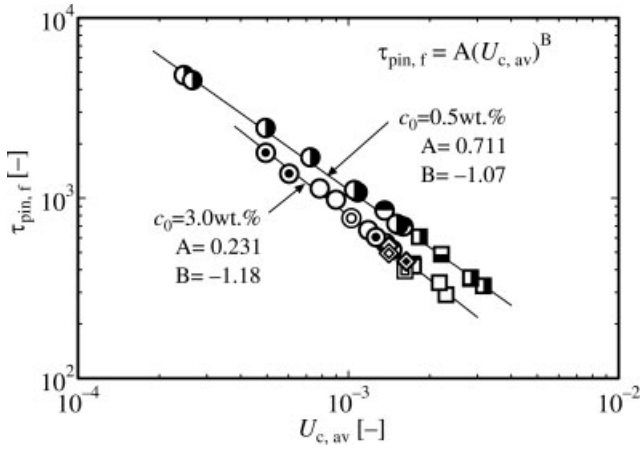

Figure 8. Normalized perimeter pinning time vs. average receding velocity.

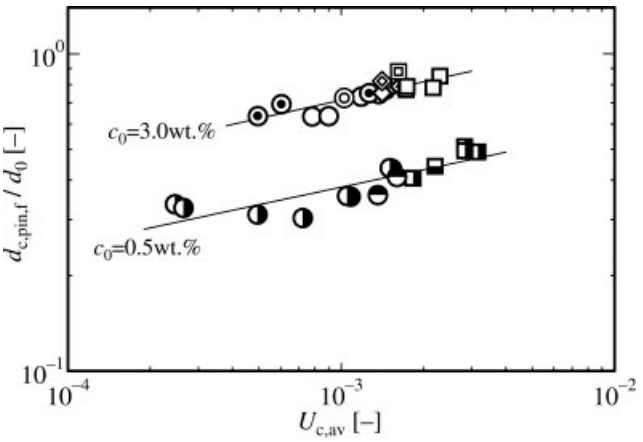

Figure 9. Diameter ratio between t = 0 and $t = t_{pin,f}$ vs. nondimensional receding velocity.

pendent of $U_{c,av}$. Therefore, a change in $c_{av,pin,f}$ with $U_{c,av}$ shows the effect of the mass diffusion during receding. As $U_{c,av}$ increases, the solute concentration at the free surface rises faster, resulting in a larger solute concentration gradient in the sessile droplet [see concentration profile scheme in Figure 11b]. As a result, $c_{av,pin,f}$ decreases as $U_{c,av}$ increases.

However, some of the solute molecules may be transported into the bulk because of free convection during the receding. Marangoni and Bénard convections in a liquid film on a heated or cooled substrate can be considered in the current system, and the critical Marangoni and Rayleigh numbers are 80[12] and 1100,[13] respectively. However, these critical values are valid for the liquid film systems, not for the droplet. Furthermore, temperatures of the substrate, the droplet and the surroundings are same and the typical definitions of these dimensionless numbers are inapplicable. Thus we first estimated these values by the definitions of Zhang and Chao.[14] They considered the temperature difference from the heat loss by the evaporation. The definitions of Ma_T and Ra_T are;

$$Ma_T = \frac{\sigma_T \dot{m} L h^2}{\mu \alpha^2 C_p}, Ra_T = \frac{\beta \rho \dot{m} L h^4}{\mu \alpha^2 C_p} \tag{6}$$

where $\sigma_T = \partial\sigma/\partial T$, $\dot{m}$, L, and h represent the surface tension due to the temperature, the evaporation rate, the latent heat, and the height of the boundary layer thickness, respectively. Assuming the constant contact angle during receding, $\dot{m}$ can be estimated as follows[15];

$$\dot{m} = \frac{\varphi(3-\phi)}{4\sqrt{\phi(2-\phi)}} u_{c,av} \tag{7}$$

where, $\varphi = 1 - \cos\psi_c$

In our case, the boundary layer thickness is presumed to the height of the droplet apex. The estimated Ma and Ra are 4-111 and 10^{-4}–10^{-2} for the present experiments. It is concluded herein that there may be a weak thermal Marangoni convection induced in the droplets under the present conditions based on these critical values. However, the effect of the solute concentration gradient over the droplet surface is not considered in the aforementioned values of Ma and Ra.

Next, Marangoni and Rayleigh numbers due to the solutal convection are estimated. Park and Moon[16] investigated the Marangoni numbers for the colloidal droplet and Cartwright et al.[17] studied for the liquid layer. These numbers are defined as follows;

$$Ma_c = \frac{\sigma_c \Delta C h}{\mu D_{AB}}, \quad Ra_c = \frac{\rho g \beta_c \Delta C h^3}{\mu D_{AB}} \tag{8}$$

where $\sigma_C = \partial\sigma/\partial C$ is the surface tension because of the concentration, ΔC the concentration difference along the convecting layer, D_{AB} represents the diffusion coefficient in binary solution, and $\beta_C = (1/\rho)(\partial\rho/\partial C)$, the volume expansion coefficient. The diffusion coefficient is obtained by the equation as follows[18];

$$D_{AB} = 7.4 \times 10^{-12} \frac{\sqrt{\phi m_B T}}{\mu_B V_A^{0.6}} \tag{9}$$

where A and B represent the solute and solvent, m_B and μ_B are the molecular weight and the viscosity of xylene, ϕ is an association factor (assumed 1) and V_A is the molar volume of polystyrene. Eq. 9 yields $D_{AB} = 1.2 \times 10^{-11}$ m^2/s for polystyrene/xylene solution. Then initial Marangoni number of 0.5 and 3.0 wt % droplet on the substrate can be estimated as $3.9 \times 10^9\ \sigma_C \Delta C$ and $1.4 \times 10^9\ \sigma_C \Delta C$. As for the solutal Rayleigh number can be estimated $1.2 \times 10^4\ \Delta C$ (0.5 wt %) and $4.2 \times 10^3\ \Delta C$ (3.0 wt %), respectively. However, the solution is prepared well-dissolved and solute concentration is almost uniform ($\Delta C \cong 0$) right after the deposition. Even though the solute distribution becomes large as the evaporation proceeds, the surface tension gradient because of the solute concentration is trivial ($\sigma_C \cong 0$) as shown in Table 1. Furthermore, the viscosity of the droplet increases during the evaporation on the substrate and then the denominators of Ra and Ma increase. Consequently, very weak thermal and solutal natural convection before the pinning of the contact line may be induced right after the deposition. However, they vanish in a moment as the evaporation proceeds, and the mass diffusion by the evaporation is dominant.

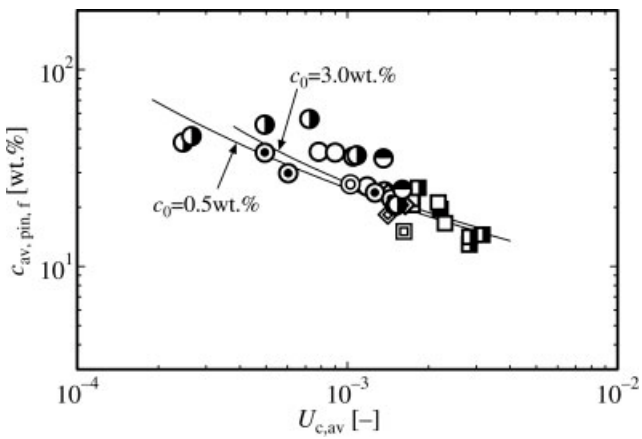

Figure 10. Average mass fraction at $t = t_{pin,f}$ vs. dimensionless receding velocity.

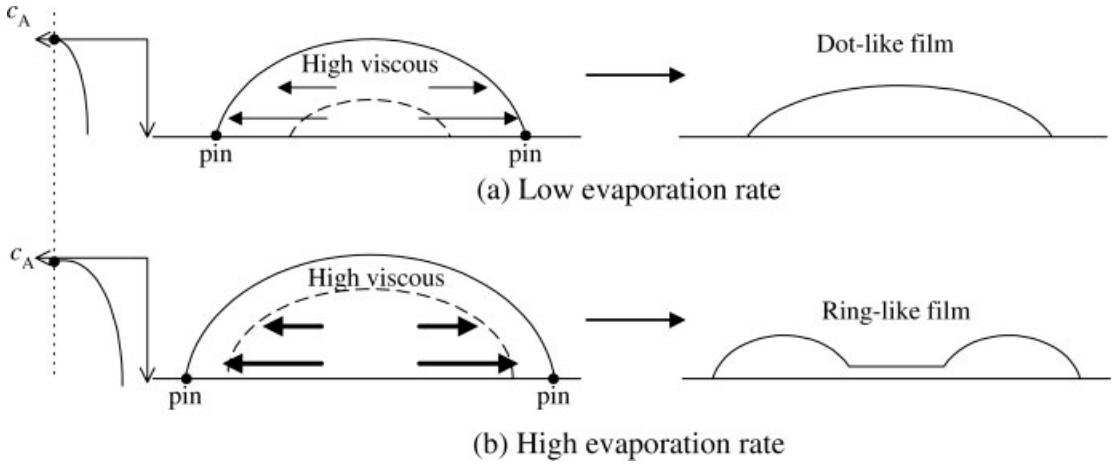

Figure 11. Schematics for formation of the dot-like and ring-like films.

The effect of the evaporation rate on film configuration

The results in Figures 8–10 suggest the followings; the contact line recedes until the solute concentration increases nearly to a critical value. When the receding velocity is high, the pinning occurs earlier and wetting diameter becomes larger with the smaller average solute concentration. In this case, ring-like film forms. Contrary, slower receding velocity induces the delayed pinning, smaller wetting diameter, and higher solute concentration with the dot-like film. These relations depend on the initial solute fraction. Above phenomena can be understood by the effect of the evaporation rate on the mass concentration.

The transition between the dot-like and ring-like films is located at $U_{c,av} = 1.5 \times 10^{-3}$ regardless of the initial droplet diameter and mass fraction. Accordingly the evaporation rate is the principle factor dominating the film configuration. As aforementioned, mass diffusion is dominant inside the droplet during receding process. At a low evaporation rate, the solute at the surface adequately diffuses into the bulk, which retards progression of solute concentration at the contact line. Therefore, the bulk solute concentration in the sessile droplet becomes higher with smaller wetting area at the pinning. After the pinning, the outward flow is induced by the non-uniform evaporation flux distribution.[9,11] However, the high concentration in the bulk prevents the solvent evaporation from the surface and outward flow due to viscous effects, resulting in a dot-like deposit [Figure 11a]. De Gans and Schubert[6] mentioned in their experimental study that a dot-like film is obtained by the binary solvent one of whose evaporation rate is much larger than the other. After the one solvent has evaporated, the residual solvent which evaporates slowly has higher concentration. This can be understood as our case of much slower evaporation rate.

Contrary for the high evaporation rate, solute at the surface cannot diffuse to the bulk, resulting in the thin high viscous area at the surface. This enhances the pinning at larger wetting diameter. The solute concentration in the bulk is lower than that for slower evaporation rate. This allows the outward flow after pinning, resulting in the ring-like deposit [Figure 11b].

Conclusion

The polystyrene/xylene droplets were ejected onto the substrate by the inkjet method, and thin films are obtained after the evaporation. The film configuration and its dominant factors are studied and we obtained the following results:

1. The heterogeneity of the receding displacement of the evaporating droplet is not dependent on the film shape. That is, the droplet center displacement during evaporation is not a dominant factor when forming the film shape.
2. The local film thickness near the periphery is governed by the local pinning time at the contact line. The heterogeneity of the local pinning time along the periphery induces the biased film.
3. During receding, a little thermal and solutal natural convection may exist right after the deposition. These convections disappear in a moment as the evaporation proceeds. Thus, the solute diffusion becomes dominant.
4. The evaporation rate of the droplet is a primary factor for the film configuration, i.e., dot-like or ring-like. A low evaporation rate yields the small dot-like film and a fast one results in the wide ring-like film. This is due to the mass transport not only after pinning but also during the receding process, predicted by the relationships of dimensionless parameters.

Acknowledgments

This study is partially supported by the Japan Society for the Promotion of Science (JSPS), Grant-in-Aid for Scientific Research (B) No. 16360387, and Ministry of Education, Culture, Sports, Science and Technology, Grant-in-Aid for Young Scientists (B) No. 17760145.

Notation

A, B = coefficients in Eq. 2
C_p = heat capacity of droplet at constant pressure, kJ/(kg·K)
c = mass fraction of solute, wt %
D = dimensionless wetting diameter, m, or diffusion coefficient, m^2/s
d = diameter, m,
h = droplet height, m
L = latent heat of droplet, kJ/kg

Ma = Marangoni number
$\dot{m}$ = evaporation rate, kg/(m^2 s)
Ra = Rayleigh number
T = temperature, K
t = time, s
U = dimensionless receding velocity = $u/u_0 = (d_0/v_0)u$
u = receding velocity, m/s
V = molar volume, m^3/mol
x = coordinate, m

Greek letters

α = thermal diffusivity, m^2/s
θ = azimuthal component, degree
μ = viscosity, kg/(m s)
ν = kinematic viscosity of fluid, m^2/s
ρ = density, kg/m^3
σ = surface tension coefficient, N/m
τ = dimensionless time = $(v_0/d_0^2)t$
ϕ = association factor in Eq. 9
ψ = contact angle, degree

Subscripts

A = solute
av = average
B = solvent
C = partial derivative by solute concentration, or solute
c = contact or wetting
g = gas
l = liquid
pin = contact line pinning
pin,f = finish of contact line pinning at whole periphery
r = receding
T = partial derivative by temperature, or temperature
0 = initial

Literature Cited

1. Hebner TR, Woo CC, Marcy D, Lu MH, Stum JC. Ink-jet printing of doped polymers for organic light emitting devices. *Appl Phys Lett*. 1998;72:519–521.
2. Bharathan J, Yang Y. Polymer electroluminescent devices processed by inkjet printing: 1. Polymer light-emitting logo. *Appl Phys Lett*. 1998;72:2660–2662.
3. Danzebrink R, Aegerter MA. Deposition of micropatterned coating using an ink-jet technique. *Thin Solid Films*. 1999;351:115–118.
4. Sirringhaus H, Kawase T, Friend RH, Shimoda T, Inbasekaran M, Wu W, Woo EP. High-resolution inkjet printing of all-polymer transistor circuits. *Science* 2000;290:2123–2126.
5. Shimoda T, Morii K, Seki S, Kiguchi H. Inkjet pringting of light—emitting polymer displays. *MRS Bull*. 2003;28:821–827.
6. de Gans BJ, Schubert US. Inkjet printing of well-defined polymer dots and arrays. *Langmuir* 2004;20:7789–7793.
7. Morita M, Koga T, Otsuka H, Takahara A. Macroscopic-wetting anisotropy on the line-patterned surface of fluoroalkylsilane monolayers. *Langmuir* 2005;21:911–918.
8. Fukai J, Ishizuka H, Sakai Y, Kaneda M, Morita M, Takahara A. Effects of droplet size and solute concentration on drying process of polymer solution droplets deposited on homogeneous surfaces. *Int J Heat Mass Transfer*. 2006;49:3561–3567.
9. Deegan RD, Bakajin O, Dupont TF, Huber G, Nagel SR, Witten TA. Capillary flow as the cause of ring stain from dried liquid drops. *Nature* 1997;389:827–829.
10. Deegan RD, Bakajin O, Dupont TF, Huber G, Nagel SF, Witten TA. Contact line deposits in an evaporating drop. *Phys Rev E*. 2000; 62:756–765.
11. Fischer BJ. Particle convection in an evaporating colloidal droplet. *Langmuir* 2002;18:60–67.
12. Pearson JRA. On convection cells induced by surface tension. *J. Fluid Mech*. 1958;4:489–500.
13. Chandrasekhar S. Hydrodynamic and Hydromagnetic Stability. New York: Dover, 1981:43.
14. Zhang N, Chao DF. Mechanisms of convection instability in thin liquid layers induced by evaporation. *Int Comm Heat Mass Trans*. 1999;26:1069–1080.
15. Utsugi H, Endo A, Suzuki N, Iikura Y. Evaporation of liquid droplets on a glass plate. *Nippon Kagaku Kaishi* 1989;9:1531–1539. (in Japanese)
16. Park J, Moon J. Control of colloidal particle deposit patterns within picolitter droplets ejected by ink-jet printing. *Langmuir* 2006;22: 3506–3513.
17. Cartwright JHE, Piro O, Villacampa AI. Pattern formation in solutal convection: vermiculated rolls and isolated cells. *Phys A*. 2002;314: 291–298.
18. Reid RC, Prausnitz JM, Sherwood TK. The Properties of Gases and Liquids, 3rd ed. New York: McGraw-Hill, 1977.

Manuscript received Feb. 19, 2006, and revision received Jan. 26, 2006.